Available online at www.sciencedirect.com
SCIENCE DIRECT®
International Journal of Heat and Mass Transfer 47 (2004) 419–428
International Journal of HEAT and MASS TRANSFER
www.elsevier.com/locate/ijhmt

Mixed convection heat and mass transfer along a vertical wavy surface

Jer-Huan Jang [a], Wei-Mon Yan [b,*]

[a] Department of Mechanical Engineering, Kuang-Wu Institute of Technology, 151 I-Der St., Pei-To, Taipei 112, Taiwan
[b] Department of Mechatronic Engineering, Huafan University, Shih Ting, Taipei 223, Taiwan

Received 27 August 2002; received in revised form 30 July 2003

Abstract

A numerical study of mixed convection heat and mass transfer along a vertical wavy surface has been carried out numerically. The wavy surface is maintained at uniform wall temperature and constant wall concentration that is higher than that of the ambient. A simple coordinate transformation is employed to transform the complex wavy surface to a flat plate. A marching finite-difference scheme is used for present analysis. The buoyancy ratio N, amplitude–wavelength ratio α, and Richardson number (Gr/Re^2) are important parameters for this problem. The numerical results, including the developments of skin-friction coefficient, velocity, temperature, concentration, Nusselt number as well as Sherwood number along the wavy surface are presented. The effects of the buoyancy ratio N and the dimensionless amplitude of wavy surface on the local Nusselt number and the local Sherwood number have been examined in detail.

1. Introduction

Many transport processes exist in nature and industrial applications in which the transfer of heat and mass occurs simultaneously as a result of combined buoyancy effects of thermal diffusion and diffusion of species. The engineering applications include the chemical distillatory processes, formation and dispersion of fog, design of heat exchangers, channel type solar energy collectors, and thermo-protection systems. Convection flows driven by temperature and concentration differences have been studied extensively in the past and various extensions of the problems have been reported in the literature. With both concentration and temperature interacting simultaneously, the convection flow can become quite complex, especially with the combination of free and force convection.

Previous studies of the flows of heat and mass convection have focused mainly on a flat plate or a regular surface. In the studies for natural convection heat and mass transfer, Bottemanne [1] had considered simultaneous heat and mass transfer by free convection along a vertical flat plate only for steady state theoretical solutions with $Pr = 0.71$ and $Sc = 0.63$. Callahan and Marner [2] studied the free convection with mass transfer on a vertical flat plate with $Pr = 1$ and a realistic range of Schmidt number. Chang et al. [3] investigated the combined buoyancy effects of thermal and mass diffusion on the natural convection flows in a vertical open tube. Yan and Lin [4] studied combined heat and mass transfer natural convection between vertical parallel plates with film evaporation. In those for mixed convection heat and mass transfer, Yan et al. [5] investigated simultaneous heat and mass transfer in laminar mixed convection flows between vertical parallel plates numerically. Lai [6] solved for coupled heat and mass transfer by mixed convection from a vertical plate in a saturated porous medium. Yan [7] studied turbulent mixed convection heat and mass transfer in a wetted channel. Kumari and Nath [8] carried out the unsteady calculation of double diffusive mixed convection flow over a vertical plate embedded in a porous medium.

The effects of mass diffusion on natural convection flows along a flat plate with different inclination have

* Corresponding author. Tel.: +886-2-26632102x2201/26633847; fax: +886-2-26633763/26633847.
E-mail address: wmyan@huafan.hfu.edu.tw (W.-M. Yan).

0017-9310/$ - see front matter © 2003 Elsevier Ltd. All rights reserved.
doi:10.1016/j.ijheatmasstransfer.2003.07.020

Nomenclature

a	amplitude of the wavy surface
c	concentration
C	dimensionless concentration
C_f	skin-friction coefficient
C_p	specific heat of fluid at constant pressure ($kJ\,kg^{-1}\,K^{-1}$)
D	mass diffusivity ($m^2\,s^{-1}$)
g	gravitational acceleration (ms^{-2})
Gr	Grashof number
k	conductivity ($W\,m^{-1}\,K^{-1}$)
L	wavelength of the wavy surface
N	buoyancy ratio, Eq. (6)
Nu	Nusselt number
P	pressure ($N\,m^{-2}$)
Pr	Prandtl number
Re	Reynolds number
Ri	Richardson number
Sc	Schmidt number
Sh	Sherwood number
T	temperature (K)
U, V	dimensionless velocity
u, v	velocity components in the x and y directions, respectively ($m\,s^{-1}$)
X, Y	dimensionless coordinate system
x, y	coordinate system (m)

Greek symbols

α	amplitude–wavelength ratio, a/L
β_T	thermal expansion coefficient
β_c	concentration expansion coefficient
μ	viscosity ($kg\,m^{-1}\,s^{-1}$)
ρ	fluid density ($kg\,m^{-3}$)
θ	dimensionless temperature
$\overline{\sigma}$	surface geometry function

Superscript

*	non-dimensional quantity

Subscripts

∞	conditions far away from the surface
c	caused by concentration
m	mean value
T	caused by temperature
w	surface condition
x	local value

been studied rather extensively. Gebhart and Pera [9], Chen and Yuh [10] and Srinivasan and Angirasa [11] investigated the effects of inclination of flat plate on the combined heat and mass transfer in natural convection. Jang and Chang [12] studied the problem of buoyancy-induced inclined boundary flows in a porous medium resulting from combined heat and mass buoyancy effects. Maughan and Incropera [13] investigated experimentally on mixed convection for air in a horizontal and inclined channel. Few studies have considered the effects of complex geometries on heat convection in micropolar fluids, including the flows along a convex surface. Wang and Kleinstreuer [14] investigated the thermal convection on micropolar fluids passing a convex with suction/injection. Yih [15] studied the heat and mass transfer characteristic in natural convection flow over a truncated cone subjected to uniform wall temperature and concentration or uniform heat and mass flux embedded in porous media. Wu et al. [16] developed a numerical model to study the effectiveness of dehydration media for wedge-shaped surface with mass and heat transfer.

It is necessary to study the heat and mass transfer from an irregular surface because irregular surfaces are often present in many applications. It is often encountered in heat transfer devices to enhance heat transfer. Mixed convection from irregular surfaces can be used for transferring heat in several heat transfer devices, for examples, flat-plate solar collectors and flat-plate condensers in refrigerators. The natural convection heat transfer from an isothermal vertical wavy surface was first studied by Yao [17,18] and using an extended Prantdl's transposition theorem and a finite-difference scheme. He proposed a simple transformation to study the natural convection heat transfer from isothermal vertical wavy surfaces, such as sinusoidal surface. Moulic and Yao [19] solved for mixed convection with thermal diffusion along a vertical wavy surface. Chiu and Chou [20] studied the natural convection heat transfer along a vertical wavy surface in micropolar fluids. Chen and Wang [21] analyzed transient free convection along a wavy surface in microfluids. Rathish Kumar et al. [22–24] presented a series of studies about the effects of phase of the wave surface on the natural convection in porous media. They found that the effects of the phase of the wavy surface on the flow and temperature fields are important. Cheng [25,26] has investigated coupled heat and mass transfer by natural convection flow along a vertical wavy surface and wavy conical surface in a porous medium. Later Wang and Chen [27] have studied transient mixed convection along a wavy surface.

Most of the previous studies about vertical wavy surfaces are concerned with microfluids or porous media. Recently, Jang et al. [28] has studied numerically

on natural convection heat and mass transfer along a vertical wavy surface. Yet the preceding literature survey shows that mixed convection heat and mass transfer in Newtonian fluid along a vertical wavy surface has not been well investigated. The objective of this study is to examine numerically the mixed convection heat and mass transfer along a vertical wavy surface by using Prandtl's transposition theorem and to investigate the effect of irregular surfaces on the characteristics of mixed convection heat and mass transfer. The numerical results, including the developments of friction factor, velocity, temperature, concentration, local Nusselt number as well as local Sherwood number along the wavy surface, are presented. The influence of Richardson number, Gr/Re^2, the buoyancy ratio N and the wavy amplitude–wavelength ratio on the local Nusselt number and Sherwood number including local skin-friction coefficient are also considered in this study.

2. Analysis

Consider a semi-infinite vertical wavy plate as shown schematically in Fig. 1. The wavy surface of the plate can be described by

$$y = \overline{\sigma}(x) = a \cdot \sin^2(\pi x/L) \tag{1}$$

where a is the amplitude of the wavy surface and L is the characteristic length of the wavy surface. The origin of the coordinate system is placed at the leading edge of the vertical surface. The surface is kept at uniform temperature T_w and uniform concentration c_w and is aligned parallel to a freestream velocity U_∞. The u and v are the velocity components in the x and y directions, respectively. The fluid oncoming to the surface has a constant temperature T_∞ and concentration c_∞. The flow is assumed to be steady and the thermal properties of the mixture are assumed to be constant except for the density variation in the buoyancy term of the momentum equation for the vertical direction.

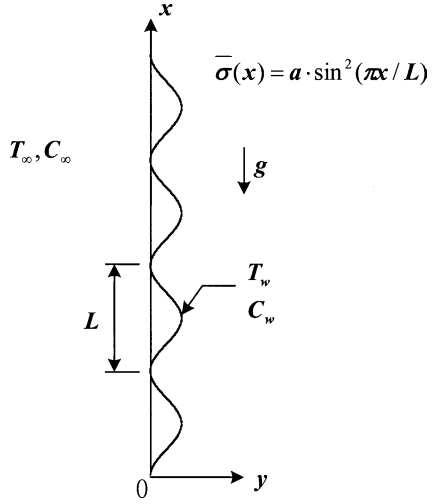

Fig. 1. Schematic diagram of the physical system.

The governing equations for a steady, laminar, and incompressible flow along a semi-infinite vertical wavy surface with Boussinesq approximation may be written as

Continuity equation

$$\frac{\partial u}{\partial x} + \frac{\partial v}{\partial y} = 0 \tag{2}$$

Momentum equation

$$\rho\left(u\frac{\partial u}{\partial x} + v\frac{\partial u}{\partial y}\right) = -\frac{\partial P}{\partial x} + \mu\left(\frac{\partial^2 u}{\partial x^2} + \frac{\partial^2 u}{\partial y^2}\right) + \rho g\beta_T(T - T_\infty) + \rho g\beta_c(c - c_\infty) \tag{3}$$

$$\rho\left(u\frac{\partial v}{\partial x} + v\frac{\partial v}{\partial y}\right) = -\frac{\partial P}{\partial y} + \mu\left(\frac{\partial^2 v}{\partial x^2} + \frac{\partial^2 v}{\partial y^2}\right) \tag{4}$$

Energy equation

$$\rho C_p\left(u\frac{\partial T}{\partial x} + v\frac{\partial T}{\partial y}\right) = k\left(\frac{\partial^2 T}{\partial x^2} + \frac{\partial^2 T}{\partial y^2}\right) \tag{5}$$

Concentration equation

$$u\frac{\partial c}{\partial x} + v\frac{\partial c}{\partial y} = D\left(\frac{\partial^2 c}{\partial x^2} + \frac{\partial^2 c}{\partial y^2}\right) \tag{6}$$

Moreover, the appropriate boundary conditions for the problem are: At the wavy surface, $u = 0$, $v = 0$, $T = T_w$, $c = c_w$; Matching with the quiescent free stream, $u = U_w(x)$, $v = 0$, $P = P_\infty(x)$, $T = T_\infty$, $c = c_\infty$, $U_w(x)$ is the x component of the inviscid velocity at the surface $y = \overline{\sigma}(x)$.

Using Prandtl's transposition theorem to transform the irregular wavy surface into a flat surface as extended by Yao [17] and boundary-layer approximation, the following dimensionless variables were introduced for non-dimensionalizing the governing equations,

$$\begin{aligned}
&x^* = \frac{x}{L}; \quad y^* = \frac{y - \overline{\sigma}}{L}Re^{1/2} \\
&u^* = \frac{u}{U_\infty}; \quad v^* = \frac{v - \sigma' u}{U_\infty}Re^{1/2}; \quad P^* = \frac{P}{\rho U_\infty^2} \\
&Re = \frac{\rho U_\infty L}{\mu}; \quad Gr = \frac{g\beta_T(T_w - T_\infty)\rho^2 L^3}{\mu^2} \\
&Pr = \frac{\mu C_p}{K}; \quad Sc = \frac{\mu}{\rho D} \\
&\theta = \frac{T - T_\infty}{T_w - T_\infty}; \quad C = \frac{c - c_\infty}{c_w - c_\infty} \\
&N = \frac{\beta_C(c_w - c_\infty)}{\beta_T(T_w - T_\infty)}; \quad \sigma = \frac{\overline{\sigma}}{L}; \ \alpha = \frac{a}{L}
\end{aligned} \tag{7}$$

It is noted that when N is equal to zero, there is no mass diffusion body force and the problem reduces to pure heat convection; when N becomes infinite, there is no thermal diffusion.

The dimensionless governing equations become

$$\frac{\partial u^*}{\partial x^*}+\frac{\partial v^*}{\partial y^*}=0 \tag{8}$$

$$u^*\frac{\partial u^*}{\partial x^*}+v^*\frac{\partial u^*}{\partial y^*}=-\frac{\partial P^*}{\partial x^*}+\sigma'\frac{\partial P^*}{\partial y^*}Re^{1/2}+(1+\sigma'^2)\times\frac{\partial^2 u^*}{\partial y^{*2}}+\frac{Gr}{Re^2}(\theta+NC) \tag{9}$$

$$u^{*2}\sigma''+\sigma'(\theta+NC)\frac{Gr}{Re^2}=\sigma'\frac{\partial P^*}{\partial x^*}-(1+\sigma'^2)\frac{\partial P^*}{\partial y^*}Re^{1/2} \tag{10}$$

$$u^*\frac{\partial \theta}{\partial x^*}+v^*\frac{\partial \theta}{\partial y^*}=\frac{1}{Pr}(1+\sigma'^2)\frac{\partial^2\theta}{\partial y^{*2}} \tag{11}$$

$$u^*\frac{\partial C}{\partial x^*}+v^*\frac{\partial C}{\partial y^*}=\frac{1}{Sc}(1+\sigma'^2)\frac{\partial^2 C}{\partial y^{*2}} \tag{12}$$

It is worth noting that the σ' and σ'' indicate the first and second differentiations of σ with respect to x^*, therefore, $\sigma'=\frac{\mathrm{d}\bar{\sigma}}{\mathrm{d}x}=\frac{\mathrm{d}\sigma}{\mathrm{d}x^*}$ and $\sigma''=\frac{\mathrm{d}\sigma'}{\mathrm{d}x^*}$. Eq. (9) shows that when $N<0$, the mass diffusion buoyancy forces oppose those of thermal diffusion, and when $N>0$, the mass diffusion buoyancy forces aid those of thermal diffusion. The Gr/Re^2 term in Eq. (10) represents the Richard number. The forced convection dominates at small values of Richardson number Ri, while natural convection takes over at large values of the same parameter. Eq. (10) indicates that the pressure gradient along the y^* axis is $\mathrm{O}(Re^{-1/2})$. This implies that the lowest-order pressure gradient along x^* axis can be determined from the inviscid flow solution and is given

$$\frac{\partial P^*}{\partial x^*}=-\left[(1+\sigma'^2)U_{\mathrm{w}}^*U_{\mathrm{w}}^{*\prime}+\sigma'\sigma''U_{\mathrm{w}}^{*2}\right] \tag{13}$$

Eliminating $\partial P^*/\partial y^*$ in Eqs. (9) and (10) resulting the following equation:

$$u^*\frac{\partial u^*}{\partial x^*}+v^*\frac{\partial u^*}{\partial y^*}=\frac{1}{1+\sigma'^2}\left[(\theta+NC)\frac{Gr}{Re^2}-\frac{\partial P^*}{\partial x^*}-u^{*2}\sigma'\sigma''\right]+(1+\sigma'^2)\frac{\partial^2 u^*}{\partial y^{*2}} \tag{14}$$

The solution has a singularity at the leading edge [19], at $x=0$, $\mathrm{d}U_{\mathrm{w}}/\mathrm{d}x$ is finite. In order to remove the singularity at the leading edge, use the following transformation:

$$X=x^*;\quad Y=y^*\left(\frac{2x^*}{U_{\mathrm{w}}^*}\right)^{-1/2}$$
$$U=\frac{u^*}{U_{\mathrm{w}}^*};\quad V=v^*\left(\frac{2x^*}{U_{\mathrm{w}}^*}\right)^{-1/2} \tag{15}$$

then Eqs. (8) and (11)–(14) could be further transformed in the parabolic coordinates (X, Y) in the following:

$$2X\frac{\partial U}{\partial X}-Y\left(1-X\frac{U_{\mathrm{w}}^{*\prime}}{U_{\mathrm{w}}^*}\right)\frac{\partial U}{\partial Y}+\frac{\partial V}{\partial Y}+2X\frac{U_{\mathrm{w}}^{*\prime}}{U_{\mathrm{w}}^*}U=0 \tag{16}$$

$$2XU\frac{\partial U}{\partial X}+\left[V-UY\left(1-X\frac{U_{\mathrm{w}}^{*\prime}}{U_{\mathrm{w}}^*}\right)\right]\frac{\partial U}{\partial Y}+2X(U^2-1)\times\left(\frac{\sigma'\sigma''}{1+\sigma'^2}+\frac{U_{\mathrm{w}}^{*\prime}}{U_{\mathrm{w}}^*}\right)=\frac{1}{1+\sigma'^2}(\theta+NC)\frac{Gr}{Re^2}\frac{2X}{U_{\mathrm{w}}^{*2}}+(1+\sigma'^2)\frac{\partial^2 U}{\partial Y^2} \tag{17}$$

$$2XU\frac{\partial \theta}{\partial X}+\left[V-UY\left(1-X\frac{U_{\mathrm{w}}^{*\prime}}{U_{\mathrm{w}}^*}\right)\right]\frac{\partial \theta}{\partial Y}=\frac{1}{Pr}(1+\sigma'^2)\frac{\partial^2\theta}{\partial Y^2} \tag{18}$$

$$2XU\frac{\partial C}{\partial X}+\left[V-UY(1-X\frac{U_{\mathrm{w}}^{*\prime}}{U_{\mathrm{w}}^*})\right]\frac{\partial C}{\partial Y}=\frac{1}{Sc}(1+\sigma'^2)\frac{\partial^2 C}{\partial Y^2} \tag{19}$$

The corresponding boundary conditions are

(1) On the wavy surface $(Y=0)$: $U=V=0$;
$\theta=1;\quad C=1$ (20)

(2) Matching with the inviscid flow $(Y\to\infty)$:
$U\to 1;\quad \theta\to 0;\quad C\to 0$ (21)

There are $U_{\mathrm{w}}^{*\prime}$ and U_{w}^* terms appeared in Eqs. (16)–(19) with the transformation. For small α, the inviscid flow solution for $U_{\mathrm{w}}^*(X)$ is

$$U_{\mathrm{w}}^*(X)=1+\alpha\left(\frac{1}{\pi}\int_0^\infty\frac{\sigma'(t)}{X-t}\mathrm{d}t\right)+\mathrm{O}(\alpha^2) \tag{22}$$

After obtaining the velocity, temperature and concentration fields along the wavy surface, the computations of the local friction coefficient, Nusselt number, and Sherwood number are of practical interest. The local heat and mass transfer rates are large when the normal velocity is approaching the surface; they are small when the convective stream moves away from the surface. The heat and mass transfer mechanism along a wavy surface is different from that along a flat surface, and is modified by the fluid motion normal to the surface. Therefore, the local Nusselt number and Sherwood number are defined respectively as

$$Nu_x=\frac{hx}{k}=\frac{\frac{\partial T}{\partial n}x}{T_{\mathrm{w}}-T_\infty}=-\left(\frac{Re_x}{2}\right)^{1/2}[(1+\sigma'^2)U_{\mathrm{w}}^*]^{1/2}\left(\frac{\partial\theta}{\partial Y}\right)_{Y=0} \tag{23}$$

$$Sh_x=\frac{h_{\mathrm{D}}x}{D}=\frac{\frac{\partial c}{\partial n}x}{c_{\mathrm{w}}-c_\infty}=-\left(\frac{Re_x}{2}\right)^{1/2}[(1+\sigma'^2)U_{\mathrm{w}}^*]^{1/2}\left(\frac{\partial C}{\partial Y}\right)_{Y=0} \tag{24}$$

where $\partial/\partial n$ represents differentiation along the normal to the surface.

The shearing stress on the wavy surface is

$$\tau_w = \left[\mu\left(\frac{\partial u}{\partial y} + \frac{\partial v}{\partial x}\right)\right]_{Y=0} \tag{25}$$

Since the local skin-friction coefficient C_{fx} is defined by

$$C_{fx} = \frac{2\tau_w}{\rho U_w^{*2}} \tag{26}$$

Substituting Eq. (25) into Eq. (26) in terms of the non-dimensional quantities, we have

$$C_{fx} = \left(\frac{1}{2Re_x}\right)^{1/2} 2(1-\sigma'^2) U_w^{*3/2} \left(\frac{\partial U}{\partial Y}\right)_{Y=0} \tag{27}$$

3. Numerical approach

In this work, a marching finite-difference scheme was used to solve the coupled governing equations for U, V, θ and C. In the transverse direction (Y), 251 non-uniform grid points were employed. Some of the calculations were tested using 501 grid points in the Y direction, but no significant improvement over the 251 grid points was found. Additionally, there are 401 grid points in the marching direction. In the program test, a finer axial step size was tried and found to give acceptable accuracy. In writing the finite-difference equations, a fully implicit numerical scheme in which the axial convection is approximated by the upstream difference and the transverse convection and diffusion terms by the central difference is used to transform the governing equations into the finite-difference equations. Each of the finite-difference equations forms a tridiagonal matrix equation, which can be efficiently solved by the Thomas algorithm [29]. To further check the adequacy of the numerical scheme used in this work, the results for the mixed convection heat transfer without concentration buoyancy in a wavy surface were first obtained. Excellent agreement between the present predictions and those of Moulic and Yao [19] was found. Through these program tests, it was found that the present numerical method is suitable for this study.

4. Results and discussion

In the present study, numerical calculations are performed for the wavy surface described by $y = \overline{\sigma}(x) = a \cdot \sin^2(\pi x/L)$ or dimensionless $\sigma(X) = \alpha \sin(\pi X)$ for amplitude–wavelength ratio of 0–0.1. In this work, the air mixture with various mass species is considered. Additionally, only the results of Richardson number Gr/Re^2 ranging from 0 to 10 are presented. From Fig. 1, it is observed that the crest of the wavy surface are at $X = 0.5, 1.5, 2.5$, etc. and while $X = 1, 2, 3$ and so on are the troughs. The velocity distribution along X-axis of this study is presented in Fig. 2. The temperature and concentration distributions are also obtained and shown in Figs. 3 and 4 respectively as well. In these figures, there are four different cases for numerical calculation, where (a) represents the typical case, and the values of α, N, and $Ri = Gr/Re^2$ are 0.05, 2, and 2 respectively; (b) represents the case of $\alpha = 0.1$, $N = 2$, and $Gr/Re^2 = 2$; (c) represents the case of $\alpha = 0.05$, $N = 2$, and $Gr/Re^2 = 10$; and (d) represents the case of $a = 0.05$, $N = 4$, and $Gr/Re^2 = 2$. For all cases, the Prantdl number and Schmidt number are held fixed at 0.7 and 1.3, respectively, throughout the calculation. The results near the leading edge of the wavy surface are not presented in these figures, because this particular position is a singular point. In Figs. 2–4, it is found that the developments of axial velocity, temperature and concentration profiles show periodical variations along the X-axis. In all cases, the amplitude of the oscillating axial velocity, temperature, and concentration decrease gradually downstream. And the axial velocity increases, while the temperature and concentration decreases along the X-axis.

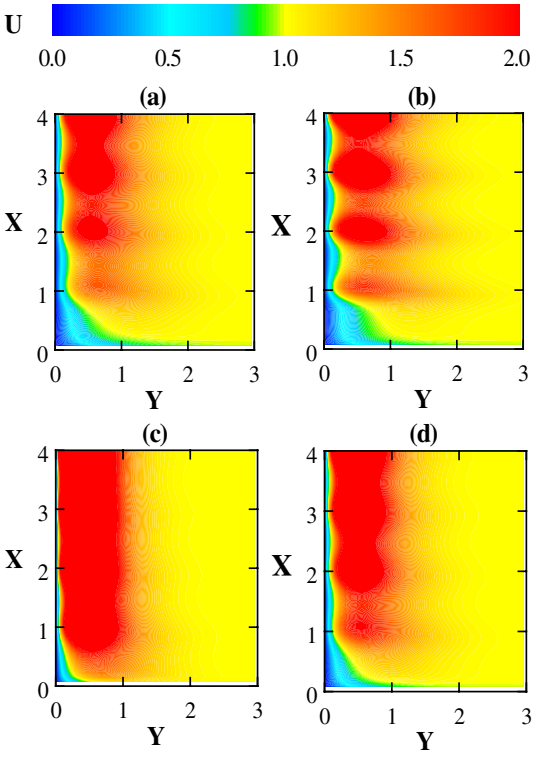

Fig. 2. The velocity contours. (a) $\alpha = 0.05$, $N = 2$, $Sc = 1.3$, $Gr/Re^2 = 2$; (b) $\alpha = 0.1$, $N = 2$, $Sc = 1.3$, $Gr/Re^2 = 2$; (c) $\alpha = 0.05$, $N = 2$, $Sc = 1.3$; $Gr/Re^2 = 10$; (d) $\alpha = 0.05$, $N = 4$, $Sc = 1.3$, $Gr/Re^2 = 2$.

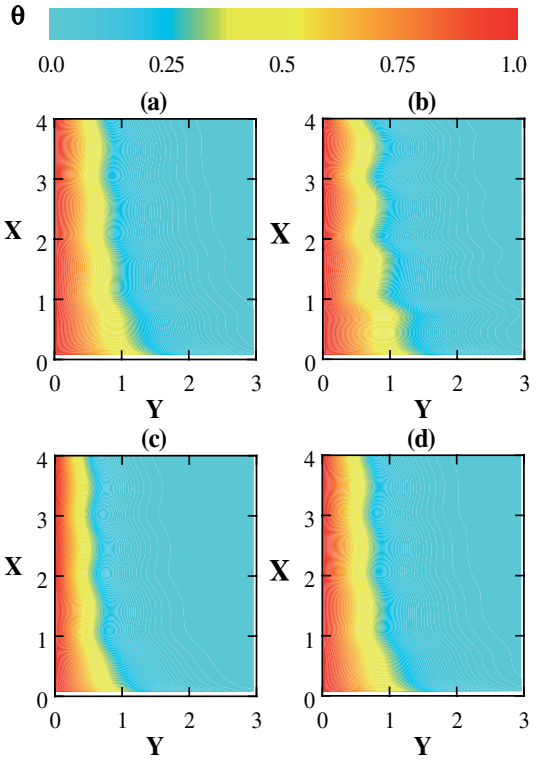

Fig. 3. The temperature contours. (a) $\alpha = 0.05$, $N = 2$, $Sc = 1.3$, $Gr/Re^2 = 2$; (b) $\alpha = 0.1$, $N = 2$, $Sc = 1.3$, $Gr/Re^2 = 2$; (c) $\alpha = 0.05$, $N = 2$, $Sc = 1.3$; $Gr/Re^2 = 10$; (d) $\alpha = 0.05$, $N = 4$, $Sc = 1.3$, $Gr/Re^2 = 2$.

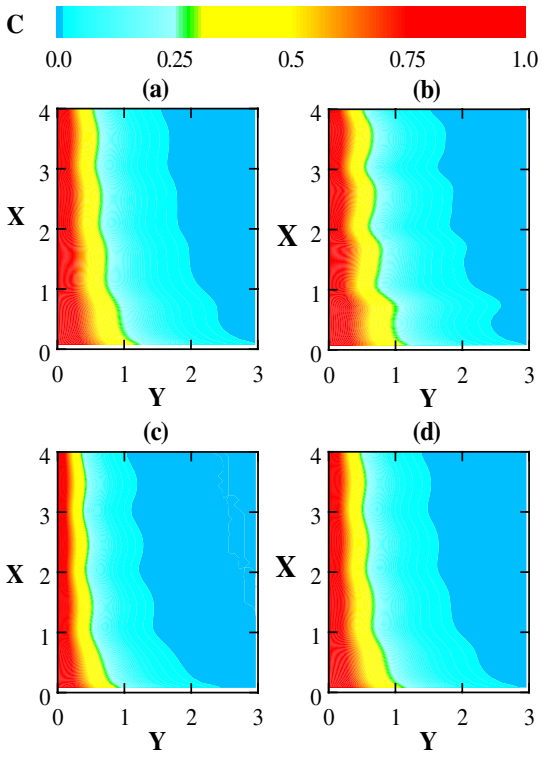

Fig. 4. The concentration contours. (a) $\alpha = 0.05$, $N = 2$, $Sc = 1.3$, $Gr/Re^2 = 2$; (b) $\alpha = 0.1$, $N = 2$, $Sc = 1.3$, $Gr/Re^2 = 2$; (c) $\alpha = 0.05$, $N = 2$, $Sc = 1.3$; $Gr/Re^2 = 10$; (d) $\alpha = 0.05$, $N = 4$, $Sc = 1.3$, $Gr/Re^2 = 2$.

In Fig. 2, the hydrodynamic boundary layer and the maximum velocity value are about the same and there occurs a periodical phenomenon for these four cases. It is obvious that the maximum velocity is greater than unity. This is due to the fact the forced flow and the buoyancy forces are in the same direction. First, comparing case (a) with case (b) in Fig. 2, the difference between these two cases is the increase of the amplitude–wavelength ratio α. It is found that there is a greater velocity fluctuation for higher amplitude–wavelength ratios. Then comparing case (a) with case (c) in Fig. 2, the only difference for these two cases is the increase in the *Ri* number. Forced convection exists as a limit when *Ri* number goes to zero and the free convection limit can be reached when *Ri* number is large. It is seen that when the Ri number increase, i.e., the convection flow is closer to free convection, the velocity distribution becomes less fluctuated. This is owing to the cumulative free convection effect. Finally, when the buoyancy ratio N is raised, by comparing cases (a) and (d) in Fig. 2, the maximum velocity range becomes large. Obviously, the contribution of mass diffusion to the buoyancy force increases the maximum velocity significantly.

In Figs. 3 and 4, the developments of temperature and concentration profiles are similar. This is due to the fact that the temperature and concentration governing equations are similar and the only difference between them is the Prantdl number *Pr* of the energy equation from the Schmidt number *Sc* of the species equation. Comparison of Figs. 3 and 4 indicates that the thermal boundary layers are thicker than those of concentration for these four cases. This is because that the Schmidt number *Sc* ($=1.3$) is greater than Prandtl number *Pr* ($=0.7$). With the comparison of cases (a) and (b) for both Figs. 3 and 4, the same result is derived with that for Fig. 2 that a higher amplitude–wavelength ratio α causes a larger fluctuation of the properties. Comparison of case (a) and case (c) reveals that both the thermal and concentration boundary layers are thicker. In these two cases, only the *Ri* number differs. The decrease of both thermal and concentration boundary layer thickness is caused by increasing the *Ri* number, which means that when the convection flow is more likely to be a free convection flow, both the thermal and concentration boundary layers become thinner. By comparing case (a) with case (d) in Figs. 3 and 4, both thermal and concentration boundary layer also are thicker. In these two

cases, the only difference is the increase of buoyancy ratio N. Therefore, the decrease of both thermal and concentration boundary layer thickness is due to the increasing buoyancy ratio.

In order to study the geometric effect on the fluid flow and heat and mass transfer, Fig. 5 shows the geometric effect on the distributions of the local skin-friction coefficient, local Nusselt number, and local Sherwood number. There is a trend observed that when the amplitude–wavelength ratio α increases for a fixed location of X-axis, the skin-friction coefficient, local Nusselt number and local Sherwood number decreases. Therefore, the heat and mass transfer rates decrease as the amplitude–wavelength ratio α increases. As go farther down the stream, the local skin-friction coefficient, local Nusselt number, and local Sherwood number increase. But there are some disturbances at higher amplitude–wavelength ratio α. It, therefore, may be concluded that the disturbance is caused by the geometric irregularity.

Fig. 6 gives the effects of buoyancy ratio N on the distributions of the local skin-friction coefficient, local Nusselt number and local Sherwood number respectively along the X-axis. It is obvious that when the buoyancy ratio N increases, the local skin-friction coefficient, local Nusselt number, and local Sherwood number increase at a given X position. It means that the buoyancy ratio enhances the heat and mass transfer of the wavy surface. This can be made plausible by noting the fact the thermal and concentration boundary layers become thinner with increasing the buoyancy ratio, and the wavy surface is kept on constant temperature and concentration, the gradients of temperature and concentration become larger. Because the heat and mass

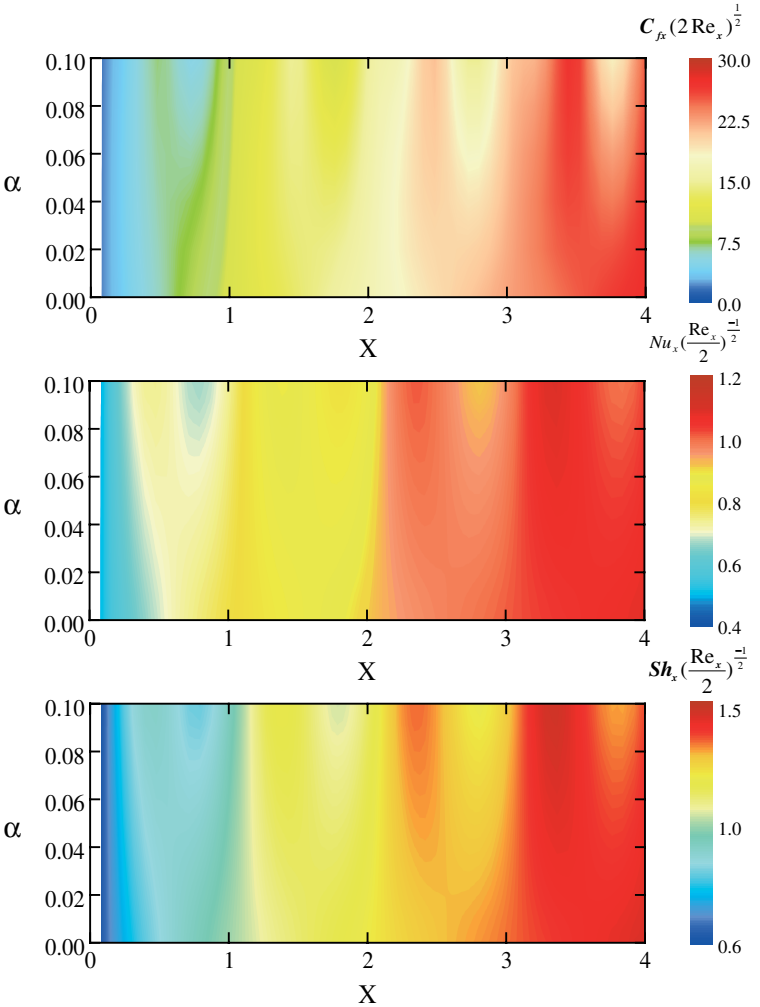

Fig. 5. Effects of amplitude–wavelength ratio α on the axial distributions of (a) local skin-friction coefficient; (b) local Nusselt number; (c) local Sherwood number.

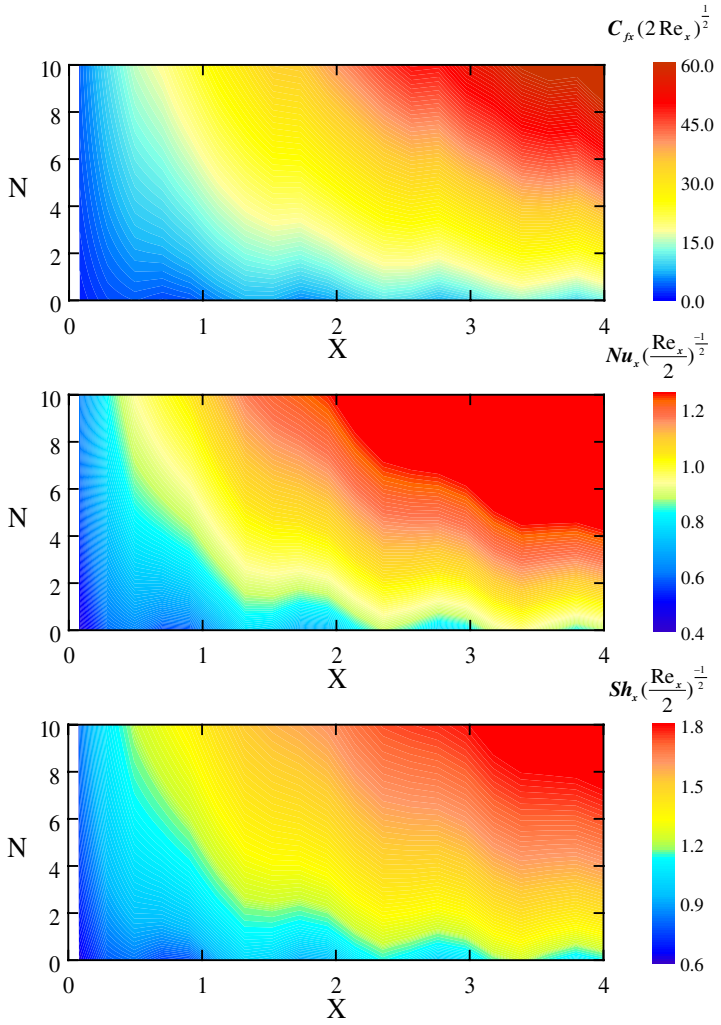

Fig. 6. Effects of buoyancy ratio N on the axial distributions of (a) local skin-friction coefficient; (b) local Nusselt number; (c) local Sherwood number.

transfer rates are proportional to the gradients of temperature and concentration, the heat and mass transfer rates are increased with the increasing buoyancy ratio N. The local skin-friction coefficient, local Nusselt number, and local Sherwood number also show fluctuation for a fixed value of N in Fig. 6. The fluctuation becomes more clearly in the downstream. This is because of the cumulative free convection effect.

Fig. 7 illustrates the influence of Richardson number Ri on the distributions of the local skin-friction coefficient, local Nusselt number, and local Sherwood number in the axial coordinate. It is seen that the skin-friction coefficient, local Nusselt number and local Sherwood number increase as Ri is raised. That is, the heat and mass transfer rate increases with increasing Richardson number Ri. When Ri increases, the buoyancy effect increases in the flow. The increasing of buoyancy effect assists the heat and mass transfer. When Ri increases, the minimum values move from the troughs to the crests. The moving of the minimum values is the influence of natural convection. Jang et al. [28] discovered that the heat and mass transfer rate has a wavelength equal to half of the wavelength of the wavy surface. When Ri increases, the flow approaches natural convection and the minimum values approach to the crest, which is consistent with the results of Jang et al. [28]. This result is also consistent with Moulic and Yao [19] that the mixed convection contains two harmonics, forced convection dominates the first harmonic is proportional to the amplitude of the wavy surface, while the natural convection is a second harmonic with a frequency twice of the wavy surface.

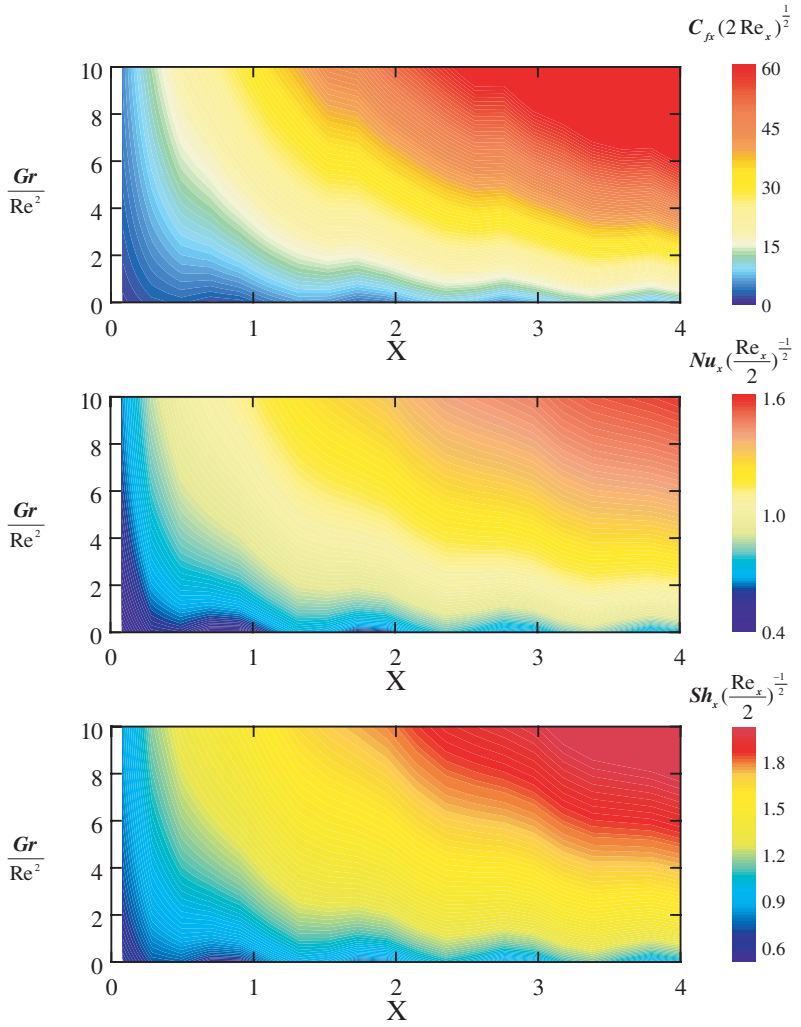

Fig. 7. Effects of mixed convection parameter Gr/Re^2 on the axial distributions of (a) local skin-friction coefficient; (b) local Nusselt number; (c) local Sherwood number.

5. Conclusions

The problem of mixed convection heat and mass transfer along a wavy surface has been analyzed. The effects of amplitude–wavelength ratio α, buoyancy ratio N, and mixed convection parameter Gr/Re^2 on momentum and heat and mass transfer have been studied in detail. Brief summaries of the major results are listed in the following:

1. The properties of the flow field for the wavy surface show a periodical variation, and the amplitude of variation decrease gradually downstream.
2. The higher amplitude–wavelength ratio increases the fluctuation of velocity, temperature and concentration fields. However, the local skin-friction, Nusselt number and Sherwood number are smaller for larger amplitude–wavelength ratios. The local skin-friction, Nusselt number and Sherwood number also increase as they go downstream.
3. The local skin-friction coefficient, Nusselt number and Sherwood number increase with an increase in the buoyancy ratio. This implies that the heat and mass transfer rates increase with the buoyancy ratio.
4. Increasing Richardson number increases the local skin-friction coefficient, Nusselt number and Sherwood number. That is, natural convection dominates over forced convection in a mixed convection flow, both heat and mass transfer rate is enhanced.
5. Mixed convection contains two harmonics, forced convection dominates the first harmonic is proportional to the amplitude of the wavy surface or near the leading edge, while free convection dominates the second harmonic or fluids move down stream.

Acknowledgements

The authors would like to acknowledge the financial support of the present work by the National Science Council, R.O.C., through the contract NSC90-2212-E-211-009.

References

[1] F.A. Bottemanne, Theoretical solution of simultaneous heat and mass transfer by free convection about a vertical flat plate, Appl. Sci. Res. 25 (1971) 137–149.
[2] G.D. Callahan, W.J. Marner, Transient free convection with mass transfer on an isothermal vertical flat plate, Int. J. Heat Mass Transfer 19 (1976) 165–174.
[3] C.J. Chang, T.F. Lin, W.M. Yan, Natural convection flows in a vertical open tube resulting from combined buoyancy effects of thermal and mass diffusion, Int. J. Heat Mass Transfer 29 (1986) 1543–1552.
[4] W.M. Yan, T.F. Lin, Combined heat and mass transfer natural convection between vertical parallel plates with film evaporation, Int. J. Heat Mass Transfer 33 (1989) 529–541.
[5] W.M. Yan, Y.L. Tsay, T.F. Lin, Simultaneous heat and mass transfer in laminar mixed convection flows between vertical parallel plates with asymmetric heating, Int. J. Heat Fluid Flow 10 (1989) 262–269.
[6] F.C. Lai, Coupled heat and mass transfer by mixed convection from a vertical plate in a saturated porous medium, Int. Commun. Heat Mass Transfer 18 (1991) 93–106.
[7] W.M. Yan, Turbulent mixed convection heat and mass transfer in a wetted channel, ASME J. Heat Transfer 117 (1995) 229–233.
[8] M. Kumari, G. Nath, Double diffusive unsteady mixed convection flow over a vertical plate embedded in a porous medium, Int. J. Energy Res. 13 (1989) 419–430.
[9] B. Gebhart, L. Pera, The nature of vertical natural convection flows resulting from the combined buoyancy effects of thermal and mass diffusion, Int. J. Heat Mass Transfer 14 (1971) 2025–2050.
[10] T.S. Chen, C.F. Yuh, Combined heat and mass transfer in natural convection on inclined surfaces, Numer. Heat Transfer 2 (1979) 233–250.
[11] J. Srinivasan, D. Angirasa, Numerical study on double-diffusion free convection from a vertical surface, Int. J. Heat Mass Transfer 31 (1988) 2033–2038.
[12] J.Y. Jang, W.J. Chang, Buoyancy-induced inclined boundary layer flow in a saturated porous medium resulting from combined heat and mass buoyancy effects, Int. Commun. Heat Mass Transfer 15 (1988) 17–30.
[13] J.R. Maughan, F.P. Incropera, Experiments on mixed convection heat transfer for air flow in a horizontal and inclined channel, Int. J. Heat Mass Transfer 30 (1987) 1307–1318.
[14] T.Y. Wang, C. Kleinstreuer, Thermal convection on micropolar fluids past two-dimensional or axisymmetric bodies with suction/injection, Int. J. Eng. Sci. 26 (1988) 1267–1277.
[15] K.A. Yih, Uniform transpiration effect on combined heat and mass transfer by natural convection over a cone in saturated porous media: uniform wall temperature/concentration or heat/mass flux, Int. J. Heat Mass Transfer 42 (1999) 3533–3537.
[16] C.H. Wu, D.C. Davis, J.N. Chung, L.C. Chow, Simulation of wedge-shaped product dehydration using mixtures of superheated steam and air in laminar flow, Numer. Heat Transfer 11 (1987) 109–123.
[17] L.S. Yao, Natural convection along a wavy surface, ASME J. Heat Transfer 105 (1983) 465–468.
[18] L.S. Yao, A note on Prandtl's transposition theorem, ASME J. Heat Transfer 110 (1988) 503–507.
[19] S.G. Moulic, L.S. Yao, Mixed convection along a wavy surface, ASME J. Heat Transfer 111 (1989) 974–979.
[20] C.P. Chiu, H.M. Chou, Transient analysis of natural convection along a vertical wavy surface in micropolar fluids, Int. J. Eng. Sci. 32 (1994) 19–33.
[21] C.K. Chen, C.C. Wang, Transient analysis of force convection along a wavy surface in micropolar fluids, J. Thermophys. Heat Transfer 14 (2000) 340–347.
[22] B.V. Rathish Kumar, P. Singh, P.V.S.N. Murthy, Effect of surface undulation on natural convection in a porous square cavity, ASME J. Heat Transfer 119 (1997) 848–851.
[23] P.V.S.N. Nurthy, B.V. Rathish Kumar, P. Singh, Natural convection heat transfer from a horizontal wavy surface in a porous enclosure, Numer. Heat Transfer 31 (Part A) (1997) 207–221.
[24] B.V. Rathish Kumar, P.V.S.N. Murthy, P. Singh, Free convection heat transfer from an isothermal wavy surface in a porous enclosure, Int. J. Numer. Methods Fluids 28 (1998) 633–661.
[25] C.Y. Cheng, Natural convection heat and mass transfer near a vertical wavy surface with constant wall temperature and concentration in a porous medium, Int. Commun. Heat Mass Transfer 27 (2000) 1143–1154.
[26] C.Y. Cheng, Natural convection heat and mass transfer near a wavy cone with constant wall temperature and concentration in a porous medium, Mech. Res. Commun. 27 (2000) 613–620.
[27] C.C. Wang, C.K. Chen, Transient force and free convection along a vertical wavy surface in micropolar fluids, Int. J. Heat Mass Transfer 44 (2001) 3241–3251.
[28] J.H. Jang, W.M. Yan, H.T. Liu, Natural convection heat and mass transfer along a vertical wavy surface, Int. J. Heat Mass Transfer 46 (2003) 1075–1083.
[29] C.V. Patankar, Numerical Heat Transfer and Fluid Flow, Hemisphere/McGraw-Hill, New York, 1980.